DOI: 10.1002/chem.201000760

Dendronizing and Metalating *trans*-2 C_{60} Tetraaryl Porphyrins—A Versatile Approach Toward Water-Soluble Donor–Acceptor Conjugates

Michaela Ruppert,[a] Fabian Spänig,[b] Mateusz Wielopolski,[b] Christof M. Jäger,[c] Walter Bauer,[a] Timothy Clark,*[c] Andreas Hirsch,*[a] and Dirk M. Guldi*[b]

Abstract: We have realized for the first time a series of truly water-soluble and tightly coupled porphyrin/C_{60} electron-donor–acceptor conjugates in which the charge separation and charge recombination dynamics are controlled by modifying the nature of the dendrimer and/or the choice of the central metal atom.

Keywords: charge transfer · fullerenes · molecular modeling · porphyrinoids

Introduction

The advent of dendronized porphyrins—also known as dendrizymes—has led to considerable attention towards testing their use as intriguing electron-transfer model systems for heme proteins (such as cytochrome c and hemoglobin).[1–14] Conjugates and/or hybrids of porphyrins and C_{60}, brought together by either covalent[15–22] or noncovalent interactions,[7,12] have emerged as outstanding photosynthetic reaction-center mimics. Because of their intrinsic features in energy and/or charge-transfer reactions, they have been replicated in the basic steps of photosynthesis, that is, light harvesting, transduction of excited state energy, charge transfer, and charge shift.[23] To this end, they have been integrated as active components into new prototypes of photovoltaic devices.[23] One of our own examples, a porphyrin/C_{60} electron-donor–acceptor conjugate (**1**) with a *trans*-2[50] addition pattern, possesses a unique face-to-face topography with the porphyrin and C_{60} moieties in van der Waals contact. The formation of **1**, starting from the corresponding bismalonate precursor, is totally regioselective because of the rigidity of the porphyrin spacer.[15]

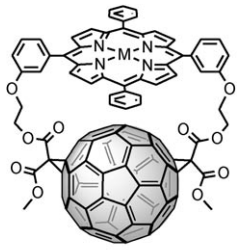

1: M = 2H, Zn

Water-soluble fullerenes are essential for many emerging biomedical technologies, which exploit the unique chemical properties and physical structure of C_{60}.[24] Moreover, they are also important for understanding the eventual fate and environmental implications of fullerenes used in consumer goods. Nevertheless, C_{60} by itself is insoluble in water, which, in turn, necessitates the development of suitable synthetic routes to overcome their hydrophobicity.[25]

The subsequent addition of the Newkome-type dendrons and the insertion of different metal atoms to porphyrins, resulted in a full-fledged family of redox-active electron-donor–acceptor conjugates with interesting charge-transfer features.[26] In the current contribution, we wish to report the development of dendronized porphyrins attached to C_{60} through a *trans*-2 addition pattern. Of utmost importance is the facile deprotection of the terminal dendritic ester groups, which, in turn, enabled a new class of truly water soluble (solubilities larger than 10 mg mL^{-1}) and tightly cou-

[a] Dipl.-Chem. M. Ruppert, Prof. Dr. W. Bauer, Prof. Dr. A. Hirsch
Department of Chemistry and Pharmacy and
Interdisciplinary Center for Molecular Materials (ICMM)
Friedrich-Alexander-Universität Erlangen-Nürnberg
Henkestrasse 42, 91054 Erlangen (Germany)
Fax: (+49) 9131-852-6864
E-mail: andreas.hirsch@chemie.uni-erlangen.de

[b] Dr. F. Spänig, Dr. M. Wielopolski, Prof. Dr. D. M. Guldi
Department of Chemistry and Pharmacy and
Interdisciplinary Center for Molecular Materials (ICMM)
Friedrich-Alexander-Universität Erlangen-Nürnberg
Egerlandstrasse 3, 91058 Erlangen (Germany)
Fax: (+49) 9131-852-7340
E-mail: dirk.guldi@chemie.uni-erlangen.de

[c] C. M. Jäger, Prof. Dr. T. Clark
Department of Chemistry and Pharmacy and
Interdisciplinary Center for Molecular Materials (ICMM)
Friedrich-Alexander-Universität Erlangen-Nürnberg
Nägelsbacherstrasse 25, 91052 Erlangen (Germany)
Fax: (+49) 9131-852-6565
E-mail: clark@chemie.uni-erlangen.de

Supporting information for this article is available on the WWW under http://dx.doi.org/10.1002/chem.201000760.

pled porphyrin/C_{60} electron-donor–acceptor conjugates to be generated.

Results and Discussion

In the quest to form dendronized *trans*-2 electron-donor–acceptor conjugates, porphyrins **2** and **3**, which contain first and second generation Newkome dendrons in the *meta* positions of the malonate-free phenyl rings, were required. Subsequent twofold cyclopropanation of these porphyrins afforded the corresponding conjugates involving a *trans*-2 addition pattern with complete regioselectivity. A common precursor of **2** and **3** is porphyrin bis-malonate **5**. To this end, porphyrin **4** was synthesized under standard Lindsey[27–29] conditions, namely, a statistical condensation of pyrrole and the corresponding benzaldehydes.

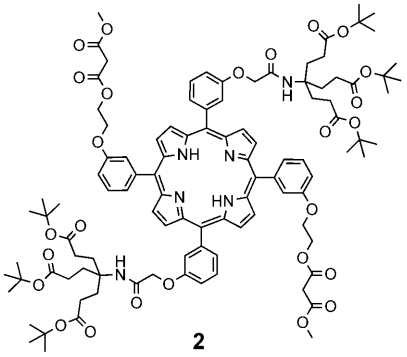

2

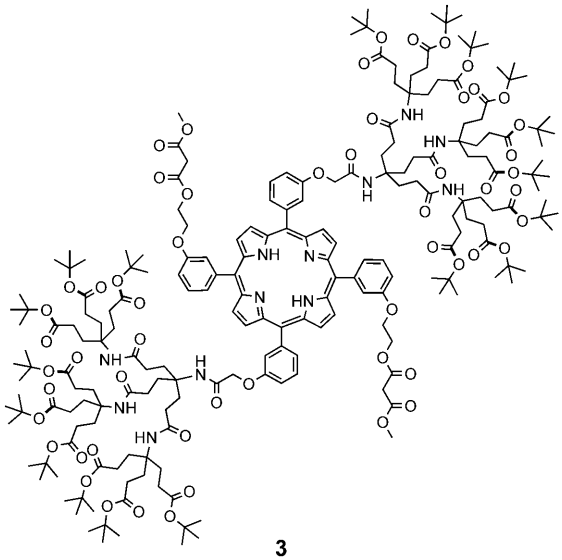

3

The co-condensation of two equivalents each of pyrrole, 3-(2-hydroxyethoxy)benzaldehyde[30] and *tert*-butyl-2-(3-formylphenoxy)acetate[31] was carried out at high dilutions, followed by oxidation with 2,3-dichloro-5,6-dicyano-1,4-benzoquinone (DDQ).

Such a statistical approach leads to the formation of a mixture of porphyrins (A_4, A_3B, A_2B_2 *cis*/*trans*, AB_3, B_4), from which the desired *trans*-substituted A_2B_2 porphyrin **4** was isolated by column chromatography on silica. The subsequent esterification with methyl-2-(chlorocarbonyl)acetate yielded porphyrin **5**, which was obtained in 90% yield after column chromatography on silica and recrystallization from *n*-pentane (Scheme 1). The next step was the formation of

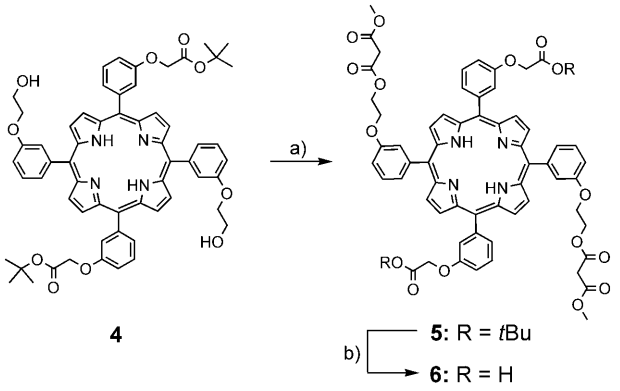

4

Scheme 1. Synthesis of porphyrins **5** and **6**. a) methyl 2-(chlorocarbonyl)acetate, pyridine, CH_2Cl_2, 0°C→RT, 90%; b) HCOOH, RT, 98%.

the free acid **6** followed by coupling to the Newkome-type dendrons H_2N-[G1] **7**[32–33] and H_2N-[G2] **8**[34] with *N*,*N*-dicyclohexylcarbodiimide (DCC) and 1-hydroxbenzotriazole (HOBt).

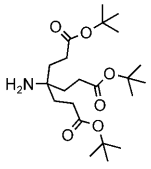

7

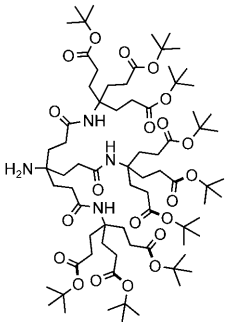

8

To remove the by-products of the reactions, the reaction mixtures were subjected to flash column chromatography on silica and precipitation from *n*-pentane. Finally, cyclopropanation of C_{60}[35–37] with the dendronized bis-malonates **2** and **3** in degassed toluene proceeded with the expected regioselectivity to afford the target compounds **H_2-9** and **H_2-10** (Scheme 2). Purification was carried out by column chromatography and recrystallization from *n*-pentane to yield the *trans*-2 conjugates in 66 and 63% yields, respectively.

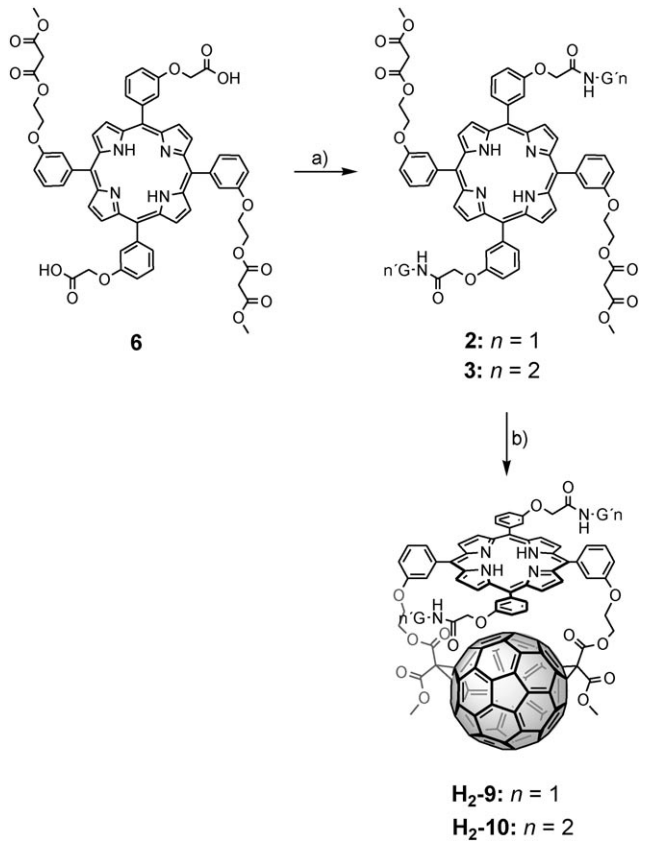

Scheme 2. Synthesis of dendronized porphyrin–fullerene dyads **H_2-9** and **H_2-10**. a) $n=1$: DCC, HOBt, DMAP, **7**, DMF, 0 °C→ RT, 51 %; $n=2$: DCC, HOBt, DMAP, **8**, DMF, 0 °C→RT, 64 %; b) $n=1$: C_{60}, I_2, **2**, DBU, toluene, RT, 66 %; $n=2$: C_{60}, I_2, **3**, DBU, toluene, RT, 63 %. G′n= number of generations ($n=1$: first generation, $n=2$: second generation).

The C_2-symmetric *trans*-2 pattern is reflected by the 26 signals in the ^{13}C NMR spectrum of **H_2-9**. In fact, two signals are of double intensity due to a total of 28 paired, chemically equivalent sp^2 atoms (i.e., C_{60}).[15] Further confirmation of the structure was provided by the presence of the four signals that relate to the carbonyl groups of the malonate unit at $\delta=163.5$ and 163.7 ppm, and to the sp^3-carbon atoms of C_{60} at $\delta=70.0$ and 70.7 ppm. Strikingly, both the *tert*-butyl and the amide NH signals appear twofold in a ratio of 1:2 in the ^1H NMR spectrum. In fact, better spectral resolution revealed a fourfold signal set in $CDCl_3$ and [D_6]DMSO.

One possible rationale, exchange tautomerism is, however, rapid at room temperature as it led to averaged signals for **H_2-9**. The pyrrole β-protons coalesce, for example, at −30 °C and 500 MHz. In principle, a hindered or slow amide rotation might be a more plausible explanation for the observed NMR signals, since *EE*, *EZ*, and *ZZ* isomers could then be observed.

Similar considerations apply for the αα, αβ, and ββ atropisomers, in which the two signals of the *EZ* isomer are expected to display identical intensities. Further insight was gained from testing an isomer of **H_2-9** in which the dendritic substituents are in the *para* rather than in the *meta* positions (see the Supporting Information). At room temperature in $CDCl_3$, the amide NH protons are seen in the form of two broadened signals in an *E*/*Z* ratio of 4:96—confirmed from an EXSY NMR spectrum—with the *ZZ* isomers prevailing.[38–40] The amide groups in **H_2-9** behave similarly. Here, the slow rotation around the C(O)–N bonds occurs in $CDCl_3$ at 22 °C with an *E*/*Z* ratio of 4:96. To conclude, we postulate for **H_2-9** a total of sixteen signal sets, however, only those of the αα, αβ, and ββ atropisomers (each with the *ZZ* configuration of the amide) are evident in the spectra (Figure 1).

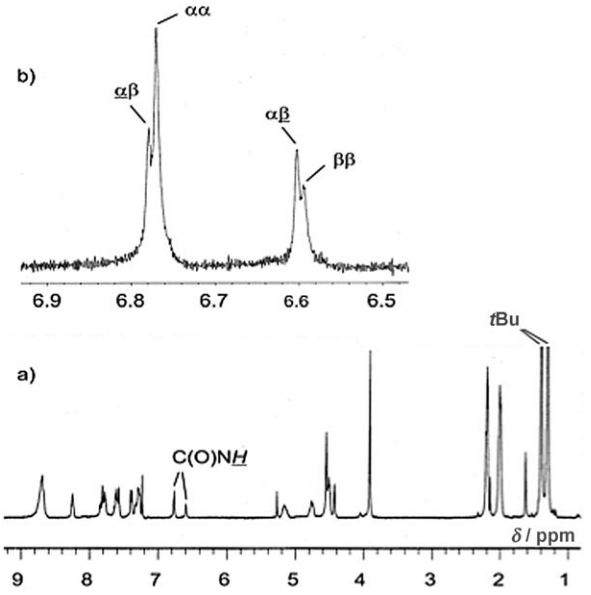

Figure 1. a) Full ^1H NMR spectrum (500 MHz, $CDCl_3$, +22 °C) of **H_2-9**. Note the presence of "two" signals each for the *tert*-butyl groups and the amide NH protons. b) Signals of the amide NH protons with resolution enhancement (Gauss window). The assignments for the atropisomers are given by αα, αβ, αβ, ββ. Note that the signals for αβ and αβ inherently must have identical intensities.

Next, NOE experiments of **H_2-9** were performed under conditions in which amide rotations and atropisomer interconversions are resolvable. At low temperatures and/or for large molecules, "NOE zero crossing" imposes difficulties in the form of the well-known negative NOE and spin diffusion.[41] Applying a "rotating frame" NOE, ROE, or a variation of ROE (DPFGSE-ROE) helped to circumvent these difficulties.[42–43] In the context of probing **H_2-9**, we chose the successive irradiation of the "two" amide NH signals, that is, low and high field. When setting the integral of the low-field amide NH resonance line to −100.0 %, a positive ROE of 4.1 % is observed for the spatially close OCH_2 protons. When exciting at the high-field amide NH resonance line, a positive ROE of 6.2 % is found for the corresponding OCH_2 group of the presumed αβ and ββ atropisomers (Figure 2).

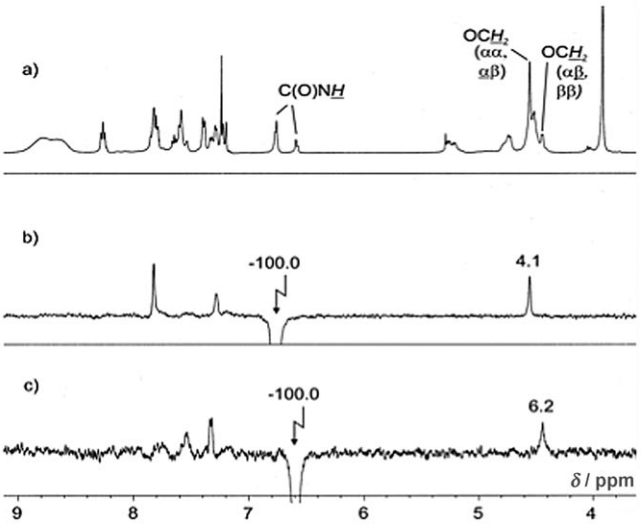

Figure 2. a) Magnified region of the ^{1}H NMR spectrum (500 MHz, $CDCl_3$, −30 °C, degassed) of **H_2-9**. b) DPFGSE-ROE spectrum of **H_2-9**, conditions as in a), selective excitation of the low-field amide NH resonance line. Numbers indicate percentage integrals, referenced to the irradiated signal = −100.0 %. Mixing time 300 ms, measuring time 7.7 h. c) same as b), selective excitation of the high-field amide NH signal.

Overall, these ROEs are of comparable magnitude. Note that amide rotamers would cause larger intensity differences in the ROE spectra.

The above observations taken together suggest that **H_2-9** gives rise to slow atropisomer interconversions (i.e., αα, αβ, ββ) as well as to slow amide rotations (i.e., *EE*, *EZ*, *ZZ*). Our analysis, however, suggests that the *ZZ* amide rotamer is the dominant species. The other amide rotamers, the *EZ* or *EE* rotamers, are present, if at all, in minor amounts. In other words, the origin of the observed "fourfold" signal set must be the atropisomers of the *ZZ*-amide rotamer with the "major" signals originating from the αα, αβ, and ββ rotamers.

The compounds **Zn^{II}-9** and **Zn^{II}-10** were obtained in very good yields by heating solutions of **H_2-9** or **H_2-10** in $CHCl_3$ with an excess of $Zn(OAc)_2 \cdot 2H_2O$.[25,44] The peripheral *tert*-butyl groups were deprotected by treating **M-9** (Scheme 3) and **M-10** (Scheme 4) with formic acid to give the hexa- and octadecacarboxylates **M-11** (M = 2H) and **M-12** (M = Zn) in quantitative yields.

The photoreactivity of **Zn^{II}-11, Zn^{II}-12, H_2-11**, and **H_2-12** was then probed in aqueous solutions at pH 7, 10, and 12. In the ground-state spectra, in addition to the porphyrin (400 and 500–600 nm) and C_{60} (300–700 nm) centered features, absorption signals were observed in the range beyond 700 nm in which neither the porphyrins nor C_{60} are known to absorb. We therefore postulate a redistribution of charge density in the ground state, that is, from the electron-donating porphyrins (i.e., $ZnP^{\delta+}$ or $H_2P^{\delta+}$) to the electron-accepting C_{60} (i.e., $C_{60}^{\delta-}$). Support for such a charge transfer came from electronic coupling matrix elements that are as high as 400 cm^{-1}. Fluorescence measurements provided a first look into the magnitude of ZnP/C_{60} or H_2P/C_{60} interactions. At

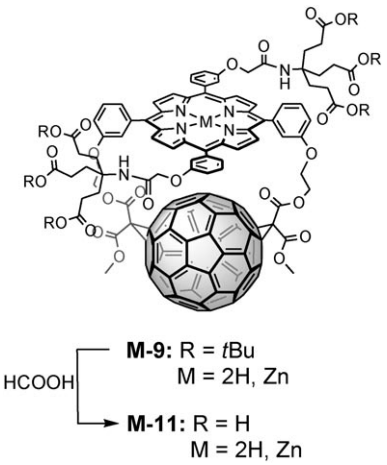

Scheme 3. Preparation of **M-11**.

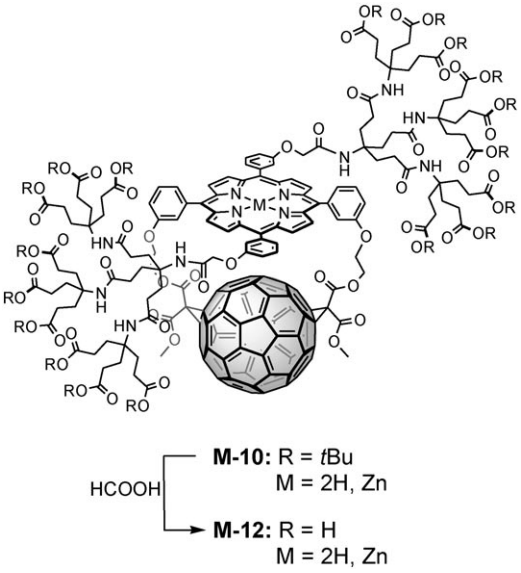

Scheme 4. Preparation of **M-12**.

any pH, sizeable interactions result in the quantitative quenching of the ZnP (i.e., $\Phi_{Em} = 0.04$) as well as H_2P (i.e., $\Phi_{Em} = 0.11$) fluorescence in **Zn^{II}-11, Zn^{II}-12, H_2-11**, and **H_2-12** (i.e., $\approx 10^{-3}$) in the 600–750 nm range and the formation of charge-transfer emission (i.e., $\approx 10^{-3}$) in the 750–850 nm range (Figure 3).

Transient absorption spectroscopy confirmed that, indeed, a charge-transfer mechanism is operative in water at any of the selected pH values. Immediately after laser excitation at 387 or 420 nm, the formation of the ZnP or H_2P singlet excited states is found for **Zn^{II}-11, Zn^{II}-12, H_2-11**, and **H_2-12**. In particular, we note characteristic absorption changes in the 500–810 and the 1000–1200 nm regions. These include a net decrease of the absorption around 540 nm, a region that is dominated by strong ZnP and H_2P ground-state absorptions.[45] Figure 4 and Figure S1 in the Supporting Informa-

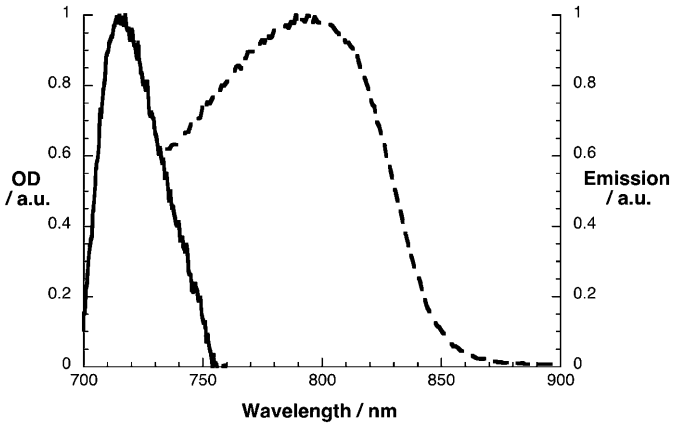

Figure 3. Charge-transfer absorption (solid line) and emission (dashed line) spectra of **H_2-11** recorded in aqueous buffer solution (pH 10) at 298 K; the excitation wavelength was 720 nm with an optical absorption of 0.06.

tion illustrate that kinetically the ZnP and H_2P singlet excited states of compounds **M-11** and **M-12** transform into new sets of maxima over the course of 2 ps, unlike the ZnP and H_2P references. Such intrinsically fast deactivations reflect the van der Waals separations between ZnP/C_{60} and H_2P/C_{60}, which are augmented by strong electronic couplings.[17,19,22]

Spectroscopically, new features evolve in the visible region (600–800 nm) and in the near-infrared region (900 nm). The close resemblance of the near-infrared part with the radiolytically and spectroelectrochemically generated spectrum of the one-electron reduced C_{60} radical anion is particularly important.[45] In the visible region, features between 600–800 nm relate to the one-electron oxidized ZnP and/or H_2P radical cations.[46–47]

Time–absorption profiles corroborate that the radical ion pair states are metastable regardless of whether ZnP (387 and 420 nm), H_2P (387 and 420 nm), C_{60} (387 nm), $ZnP^{\delta+}$-$C_{60}^{\delta-}$ (charge-transfer (CT) absorption), or $H_2P^{\delta+}$-$C_{60}^{\delta-}$ (CT absorption) are excited. An interesting observation is that the pH has no effect on the stability of $ZnP^{\bullet+}$-$C_{60}^{\bullet-}$ and $H_2P^{\bullet+}$-$C_{60}^{\bullet-}$. But, unlike the assays in organic solvents (see below) the decay depends strongly on the dendrimer generation and is multi-exponential. Two components are needed to describe the $H_2P^{\bullet+}$-$C_{60}^{\bullet-}$ dynamics for **H_2-11** (135 and 950 ps), **H_2-12** (50 and 520 ps), **Zn^{II}-11** (6 and 50 ps), and **Zn^{II}-12** (25 and 275 ps).[48] These results imply that different, concurrently formed $MP^{\bullet+}$-$C_{60}^{\bullet-}$ species with varying stability are formed. A possible rationale involves the role of the different dendrimer rotamers (i.e., first and second generation) as the NMR spectral characterizations suggest.

This led us to reexamine **Zn^{II}-9, Zn^{II}-10, H_2-9**, and **H_2-10** by time-resolved transient absorption spectroscopy in organic solvents, exciting the samples at 387 or 420 nm. Throughout the visible and near-infrared regions, the ZnP and H_2P singlet excited state fingerprints are discernable. The presence of C_{60}, nevertheless, causes a nearly instantaneous decay of the ZnP and H_2P singlet excited states. As the singlet features fade, the signatures of the $ZnP^{\bullet+}$-$C_{60}^{\bullet-}$ and $H_2P^{\bullet+}$-$C_{60}^{\bullet-}$ radical ion pair states arise in the visible (600–800 nm) and near-infrared (900 nm) regions. Likewise, exciting the charge-transfer features, into the maximum of the CT absorption, causes these to convert into those of the $ZnP^{\bullet+}$-$C_{60}^{\bullet-}$ and $H_2P^{\bullet+}$-$C_{60}^{\bullet-}$ radical ion pair states (Figure S2 in the Supporting Information). In organic solvents, the decays of the radical ion pair states are strictly monoexponential and result in the quantitative regeneration of the ground states.[17,19] Two factors (i.e., the nature of the donor and solvent polarity) govern the dynamics. The longest lifetimes are found, for example, for $H_2P^{\bullet+}$-$C_{60}^{\bullet-}$ in toluene (2200 ps for **H_2-9** and **H_2-10**), whereas $ZnP^{\bullet+}$-$C_{60}^{\bullet-}$ exhibits generally shorter lifetimes (375 ps in toluene for **Zn^{II}-9, Zn^{II}-10**) and the shortest value in DMF (25 ps for **Zn^{II}-9, Zn^{II}-10**).[49] These values are in line with charge separation and charge recombination dynamics in the Marcus-normal and the Marcus-inverted regions, respectively.

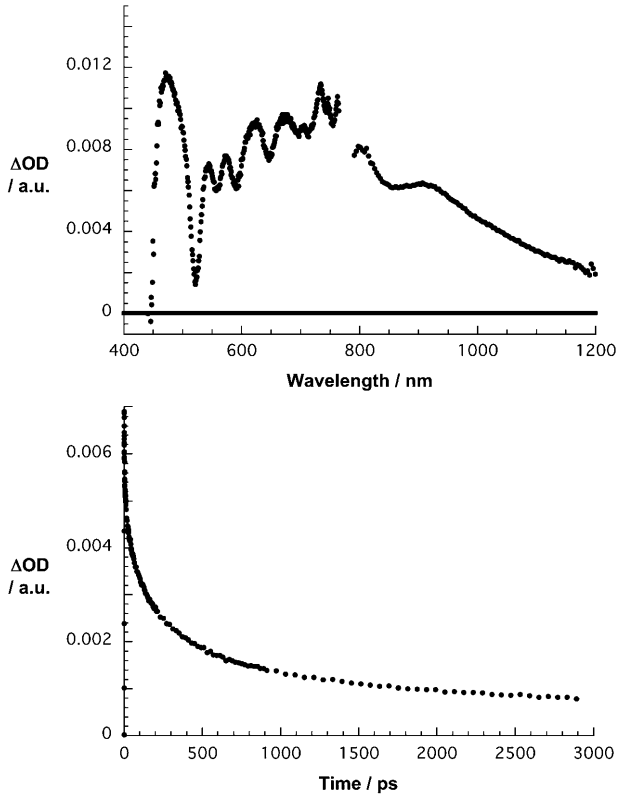

Figure 4. Top: differential absorption spectra (visible and near-infrared) obtained upon femtosecond flash photolysis (420 nm, 100 nJ) of **H_2-11** ($\approx 10^{-6}$ M) in argon saturated H_2O (pH 10) with a time delay of 5 ps at room temperature. Bottom: time versus absorption profile at 900 nm of the spectra shown above, monitoring the charge separation and charge recombination.

Using the above information for **Zn^{II}-9, Zn^{II}-10, H_2-9**, and **H_2-10**, we employed the relationship of radical ion pair state lifetime, for the recovery of the ground state, versus polarity to assess the solvent environment that the different dendrimer generations create in **Zn^{II}-11, Zn^{II}-12, H_2-11**, and **H_2-12** (Figure 5).

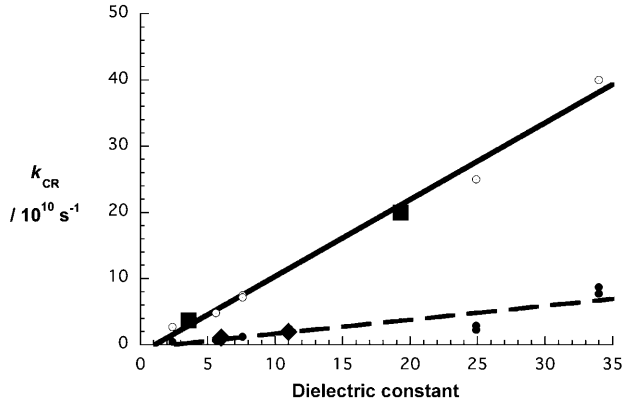

Figure 5. Dependence of dielectric constant versus charge recombination rate constants in **Zn^{II}-9**, **Zn^{II}-10** (○, solid line), **H_2-9**, and **H_2-10** (●, dashed line) to evaluate the environment of **Zn^{II}-11**, **Zn^{II}-12** (■), **H_2-11**, and **H_2-12** (◆).

In doing so, we relate the long lifetime components to polarities of 3.6 (i.e., $ZnP^{\bullet+}$-$C_{60}^{\bullet-}$ in **Zn^{II}-11**), 19.3 (i.e., $ZnP^{\bullet+}$-$C_{60}^{\bullet-}$ in **Zn^{II}-12)**, 6 (i.e., $H_2P^{\bullet+}$-$C_{60}^{\bullet-}$ in **H_2-11**), and 11 (i.e., $H_2P^{\bullet+}$-$C_{60}^{\bullet-}$ in **H_2-12**). To address the question as to why the first-generation dendrimer is apparently linked with a better stabilization/lower "apparent" dielectric constant than the second generation, we turned to quantum chemical calculations. Geometry optimizations suggest that the shielding effects of the electroactive moieties vary in the different conformers. The latter also affects the charge separation and charge recombination dynamics. Due to the fact that the photophysical studies were carried out in aqueous solution, we have performed the molecular dynamics simulations in an aqueous environment to shed light on the conformational dynamics of **Zn^{II}-11** and **Zn^{II}-12**.

These simulations reveal that atropisomerism is maintained in both **Zn^{II}-11** and **Zn^{II}-12**, so that the atropisomers are stable over the period of the simulations in water. Moreover, the position of the dendrimer relative to ZnP strongly depends on the generation. In **Zn^{II}-11**, the preferred conformation brings both dendrimers above the ZnP plane and, in turn, shields the latter. The distance between the mean porphyrin plane and central amide nitrogen atoms of the dendrimer was used to characterize the conformations (Figure 6). In stark contrast, the size and the number of negative charges of the dendritic arms in **Zn^{II}-12** ensures interactions with ZnP and C_{60} in virtually all isomers. No preference for either ZnP or C_{60} shielding was, however, seen throughout the entire simulation. Due to the high flexibility of the second-generation dendrimer and the resulting interactions with the hydrophobic sites, the formation of a cagelike protecting shield around the molecule was found. The compact arrangement forces donor–acceptor center-to-center distances of around 6.0 Å. Interestingly, this electron-donor–acceptor distance is decreased by 1.0 Å relative to that in **Zn^{II}-11**. The atropisomerism in **Zn^{II}-12** has no appreciable impact on the relative conformation of the dendrimers with respect to the ZnP plane. Shielding of ZnP or C_{60} may thus occur independently of the position of the nitrogen atoms relatively to the ZnP plane (Figure 7). Due to the increased mean distance between the amide nitrogen atoms and the ZnP plane, by almost 2 Å, the formation of the cagelike protecting shield around the whole molecule occurs at the expense of shielding effects of the individual electroactive moieties, that is, ZnP and C_{60}.

Finally, to corroborate the concept of different shielding effects rather than formation of micellar structures, conductivity and dynamic light scattering (DLS) measurements were carried out with **H_2-11**, **Zn^{II}-11**, **H_2-12**, and **Zn^{II}-12** (Figure S6 in the Supporting Information). Since the conductivity scales linearly with concentration, micellar aggregation is ruled out. Likewise, the volume density distribution of **Zn^{II}-11** and **Zn^{II}-12** in a concentration range from 10^{-6} to 10^{-4} M at pH 10 identifies the monomeric species (Figure S7 in the Supporting Information).

Conclusion

We have realized for the first time a series of truly water-soluble, tightly coupled porphyrin/C_{60} electron-donor–acceptor conjugates through tether-controlled synthesis and facile, covalent introduction of Newkome-type dendrimers. Full control over the charge-transfer chemistry, that is, charge separation and charge recombination dynamics, is achieved by modifying the nature of the dendrimer and/or the choice of the central metal. Stabilization of the radical ion pair states is maximized in **H_2-11** upon 1) the shielding of the most susceptible moieties (i.e., H_2P/ZnP versus C_{60}), 2) the larger donor–acceptor separation (i.e., first versus second generation dendrimers), and 3) the use of the weaker electron donor (i.e., H_2P versus ZnP), whereas micellar aggregation has been excluded. From a broader perspective, we hope that our finding will provide the impetus for probing charge-transfer-induced reactions with C_{60} and related fullerenes under biologically relevant conditions.

Experimental Section

General remarks and experimental procedures are given in the Supporting Information.

Compound 4: 3-(2-hydroxyethoxy)benzaldehyde (10 g, 60 mmol), *tert*-butyl-(2,3-formylphenoxy)acetate (14 g, 60 mmol), pyrrole (8.50 mL, 120 mmol), PPh_4Cl (157 mg, 0.40 mmol), and ethanol (20 mL) were dissolved in CH_2Cl_2 (3.50 L). After addition of $BF_3{\cdot}Et_2O$ (1.50 mL, 12 mmol) the solution was stirred for 30 min. DDQ (20 g, 90 mmol) was added, the solution was stirred for 1 h, and the solvent was removed by distillation. The crude mixture was purified by passing through a silica plug and adjacent multiple column chromatography (SiO_2, CH_2Cl_2/EtOAc 8:2). The product was obtained as a violet solid in 2.70% yield (820 mg). ^{1}H NMR (400 MHz, RT, $CDCl_3$): $\delta = -2.80$ (br, 2H; NH), 1.40 (s, 18H; *t*Bu), 4.05 (s, 4H; CH_2), 4.34 (s, 4H; CH_2), 4.74 (s, 4H; CH_2), 7.33–7.88 (m, 16H; Ar-H), 8.96 ppm (br, 8H; β-H); ^{13}C NMR (100.5 MHz, RT, $CDCl_3$): $\delta = 28.0$ (*t*Bu), 61.5 (CH_2), 65.7 (CH_2), 69.4 (CH_2), 82.4 (qC), 113.8, 114.1, 114.4 (Ar-C), 119.6, 119.7, 120.9, 121.1 (*meso*-C), 127.6, 128.0, 128.4, 129.7 (Ar-C), 131.2 (β-C), 143.4, 143.5, 156.3, 157.0 (Ar-C), 168.0 ppm (C=O); IR (ATR): $\tilde{\nu} = 713$, 746, 774, 789,

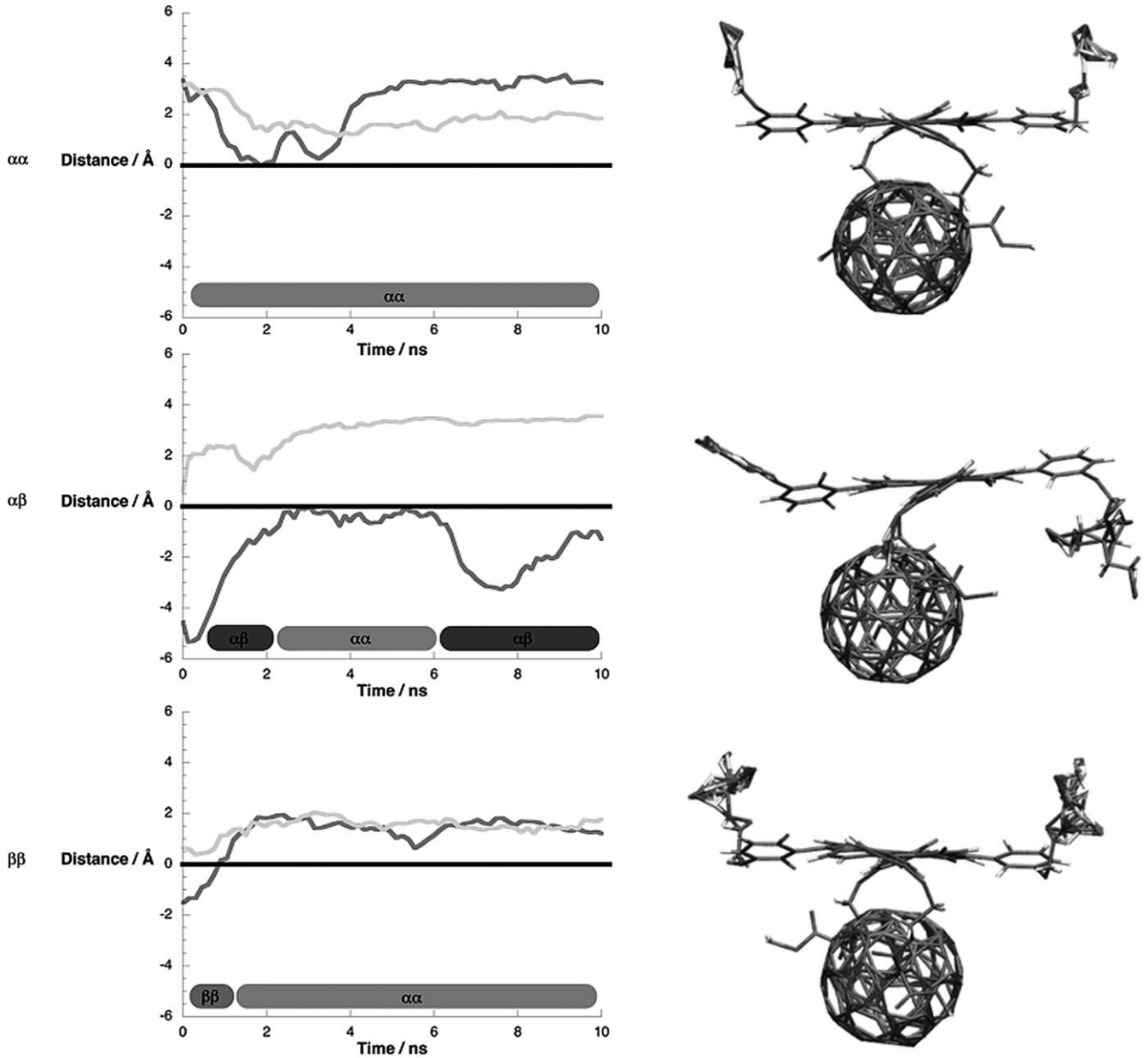

Figure 6. Relative position (i.e., the distance of the dendrimer's central amide nitrogen atoms to the ZnP plane) of the dendritic side chains towards the porphyrin as a function of time in **Zn^{II}-11** (left). Corresponding average structures are displayed as insets (right).

801, 978, 1044, 1083, 1153, 1233, 1287, 1383, 1474, 1574, 1605, 1735, 2341, 2361, 2878, 2944, 2971, 3489 cm^{-1}; UV/Vis (CH_2Cl_2): λ (log ε) = 419 (5.48), 515 (4.18), 550 (3.77), 589 (3.77), 642 nm (3.46); MS (FAB, NBA): *m*/*z*: 995 [M^+], 939 [M^+−*t*Bu], 883 [M^+−2*t*Bu].

Compound 5: Compound **4** (820 mg 0.83 mmol) and pyridine (167 μL, 2.08 mmol) were dissolved in CH_2Cl_2 (350 mL). The mixture was cooled in an ice bath and a solution of (218 μL, 2.08 mmol) in CH_2Cl_2 (40 mL) was added dropwise. After stirring for 12 h the solution was washed with water, dried over $MgSO_4$, and purified by column chromatography (SiO_2, CH_2Cl_2/EtOAc 9:1). After recrystallization from *n*-pentane the product was isolated as a violet solid in 90% (890 mg) yield. ^{1}H NMR (400 MHz, RT, $CDCl_3$): δ = −2.80 (br, 2H; NH), 1.45 (s, 18H; *t*Bu), 3.56 (s, 4H; CH_2), 3.83 (s, 6H; OCH_3), 4.47 (m, 4H; CH_2), 4.41 (m, 4H; CH_2), 4.74 (s, 4H; CH_2), 7.33–7.78 (m, 16H; Ar-H), 8.96 ppm (br, 8H, β-H); ^{13}C NMR (100.5 MHz, RT, $CDCl_3$): δ = 28.0 (*t*Bu), 41.1 (CH_2), 52.6 (OCH_3), 63.8 (CH_2), 65.7 (CH_2), 65.8 (CH_2), 82.4 (qC), 114.2, 114.3, 114.4 (Ar-C), 118.5, 119.6, 120.8, 121.1 (*meso*-C), 127.6, 128.1, 128.4 (Ar-C), 131.4 (β-C), 143.4, 143.5, 156.3, 156.7 (Ar-C), 166.5, 166.8, 168.0 ppm (C=O); IR (ATR): $\tilde{\nu}$ = 735, 778, 805, 915, 976, 1076, 1152, 1228, 1349, 1368, 1436, 1578, 1579, 1737, 2341, 2360, 2970, 3320 cm^{-1}; UV/Vis (CH_2Cl_2): λ (log ε) = 420 (5.40), 514 (4.10), 549 (3.74), 590 (3.67), 645 nm (3.49); MS (FAB, NBA): *m*/*z*: 1195 [M^+], 1139 [M^+−*t*Bu], 1083 [M^+−2*t*Bu].

Compound 6: Compound **5** (890 mg, 0.74 mmol) was stirred overnight in formic acid. After evaporation of the formic acid, the product was obtained in 99% yield. ^{1}H NMR (400 MHz, RT, [D_8]THF): δ = −2.72 (br, 2H; NH), 3.42 (s, 4H; CH_2), 3.83 (s, 6H; OCH_3), 4.38 (m, 4H; CH_2), 4.51 (m, 4H; CH_2), 4.82 (s, 4H; CH_2), 7.37 (m, 4H; Ar-H), 7.65 (m, 4H; Ar-H), 7.82 (m, 8H; Ar-H), 8.96 ppm (m, 8H; β-H); ^{13}C NMR (100.5 MHz, RT, [D_8]THF): δ = 41.3 (CH_2), 52.2 (OCH_3), 64.3 (CH_2), 65.5 (CH_2), 66.9 (CH_2), 115.0, 115.3 (Ar-C), 120.5, 120.7, 121.7, 121.8

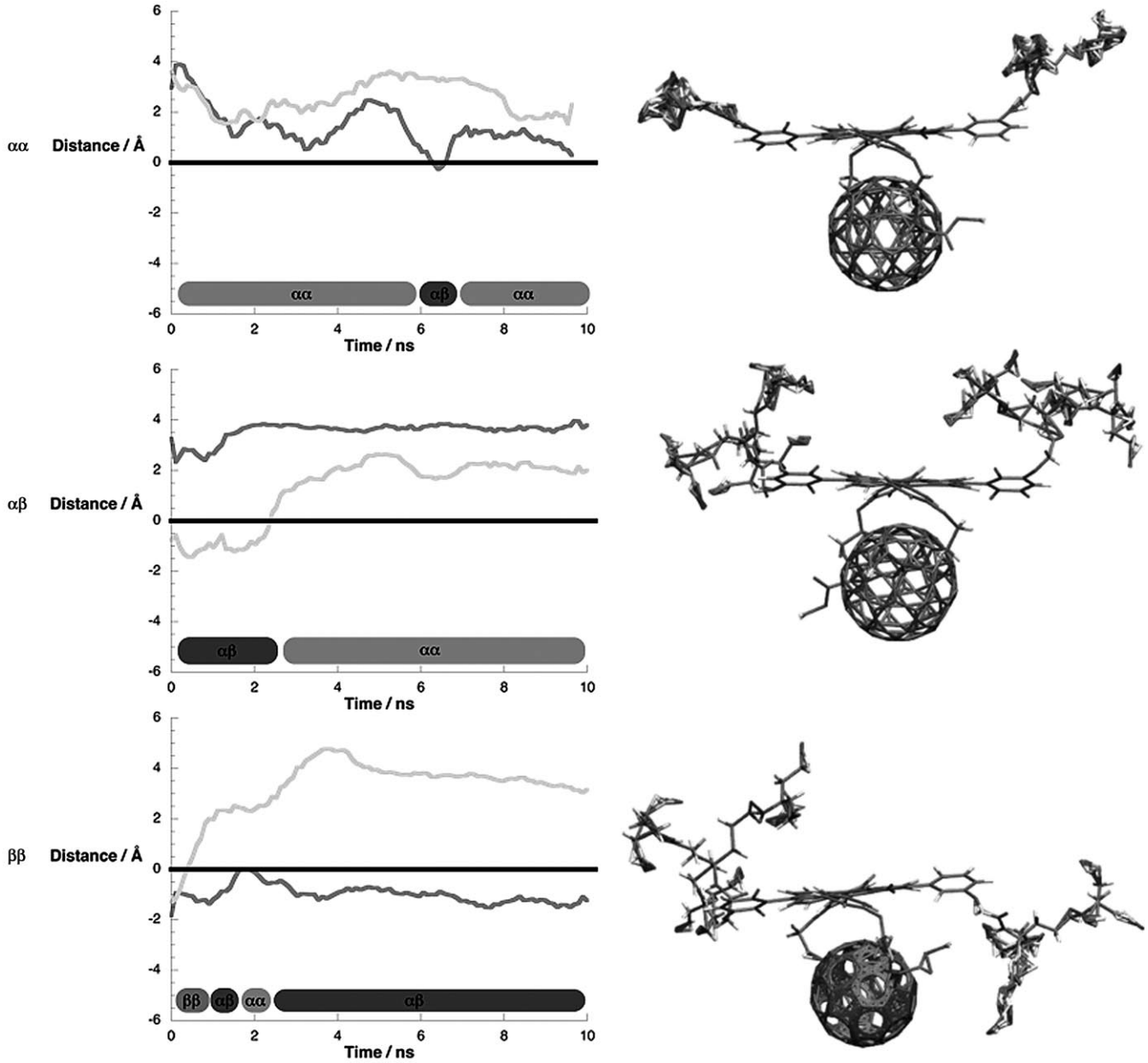

Figure 7. Relative position (i.e., the distance of the dendrimer's central amide nitrogen atoms to the ZnP plane) of the dendritic side chains towards the porphyrin as a function of time in **Zn^{II}-12** (left). Corresponding average structures are displayed as insets (right).

(*meso*-C), 128.2, 128.4, 128.7, 128.8 (Ar-C), 131.3 (β-C), 144.2, 144.5, 157.9, 158.2 (Ar-C), 167.0, 167.2, 170.2 ppm (C=O); IR (ATR): $\tilde{\nu}$ = 735, 796, 900, 1216, 1228, 1365, 1435, 1507, 1738, 2341, 2360, 2970, 3015 cm^{-1}; UV/Vis (THF): λ (log ε) = 417 (5.56), 513 (4.27), 548 (3.93), 592 (3.75), 643 nm (3.75); MS (FAB, NBA): *m*/*z*: 1083 [M^+].

Compound 2: Compound **6** (400 mg, 0.37 mmol) was dissolved in DMF (150 mL). After cooling the solution in an ice bath, DCC (305 mg, 1.48 mmol), HOBt (200 mg, 1.48 mmol), and DMAP (9 mg, 0.08 mmol) were added. The mixture was stirred for 1 h before **7** (460 mg, 1.11 mmol) was added. After stirring for 24 h, the solvent was removed by distillation and the residue dissolved in ethyl acetate. Precipitated DCU was removed by filtration and the solution was washed with 10% citric acid solution, a solution of $NaHCO_3$ (8%), brine, and water and dried over $MgSO_4$. Adjacent column chromatography (SiO_2, CH_2Cl_2/ethyl acetate 8:2) gave the wine red product in 51% (360 mg) yield. ^{1}H NMR (400 MHz, RT, $CDCl_3$): δ = −2.81 (br, 2H; NH), 1.35 (s, 54H; *t*Bu), 2.05 (m, 12H; CH_2), 2.25 (m, 12H; CH_2), 3.46 (s, 4H; CH_2), 3.69 (s, 6H; OCH_3), 4.39 (s, 4H; CH_2), 4.58 (s, 4H; CH_2), 4.61 (s, 4H; CH_2), 6.81 (s, 2H; NH(C=O)), 7.33–7.88 (m, 16H; Ar-H), 8.87 ppm (m, 8H; β-H); ^{13}C NMR (100.5 MHz, $CDCl_3$, RT): δ = 28.0 (*t*Bu), 29.7, 30.0 (CH_2), 41.1 (CH_2), 52.5 (OCH_3), 57.6 (CH_2), 63.8 (CH_2), 65.8 (CH_2), 67.5 (CH_2), 80.6 (^{q}C), 113.7, 114.3 (Ar-C), 119.3, 119.8, 121.0, 121.7 (*meso*-C), 127.6, 127.8, 128.2, 128.9 (Ar-C), 131.1 (β-C), 143.5, 143.8, 155.5, 156.2, 156.7 (Ar-C), 166.5, 166.7, 167.1, 172.5 ppm (C=O); IR (ATR): $\tilde{\nu}$ = 777, 804, 847, 918, 997, 1101, 1150, 1216, 1229, 1366, 1435, 1524, 1599, 1736, 2341, 2361, 2970 cm^{-1}; UV/Vis (CH_2Cl_2): λ (log ε) = 419 (5.56), 513 (4.24), 548 (3.90), 591 (3.75), 645 nm (3.75); MS (FAB, NBA): 1876 [M^+−2H], 1820 [M^+−*t*Bu].

Compound H_2-9: C_{60} (123 mg, 0.17 mmol) was dissolved in toluene (300 mL) and degassed with argon for 15 min. Compound **2** (207 mg, 0.11 mmol) and iodine (112 mg, 0.44 mmol) were then added. A solution of DBU (66 μL, 0.44 mmol) in toluene (15 mL) was added dropwise and the mixture was stirred for 2 d. The solution was concentrated and the crude product was purified by column chromatography (SiO_2, toluene/ethyl acetate 7:3). After recrystallization from *n*-pentane the product was obtained as a brown solid in 66% yield (190 mg). ^{1}H NMR (400 MHz, RT, $CDCl_3$): $\delta = -3.04$ (br, 2H; NH), 1.31 (s, 36H; *t*Bu), 1.41 (s, 18H; *t*Bu), 2.00 (m, 12H; CH_2), 2.20 (m, 12H; CH_2), 3.91 (s, 6H; OCH_3), 4.55 (m, 8H; CH_2), 4.78 (m, 2H; CH_2), 5.27 (m, 2H; CH_2), 6.81 (m, 2H; NH-(C=O)), 7.28–7.83 (m, 16H; Ar-H), 8.69 ppm (m, 8H; β-H); ^{13}C NMR (100.5 MHz, RT, $CDCl_3$,): $\delta = 28.0$, 28.1 (*t*Bu), 29.6, 29.9 (CH_2), 49.1 (CH_2), 53.9 (OCH_3), 57.6 (^{q}C), 65.0 (CH_2), 67.3 (CH_2), 67.4 (CH_2), 70.0, 70.7 (C_{60}-sp^3), 80.6 (^{q}C), 113.5, 115.4 (Ar-C), 119.5, 119.9, 121.0, 121.6 (*meso*-C), 123.8, 126.9, 127.8, 128.7 (Ar-C), 130.9 (β-C), 138.0, 138.1, 138.3, 139.0, 139.1, 139.7, 139.8, 139.9, 140.5, 140.6, 140.8, 141.0, 141.1, 141.3, 141.5, 141.6, 141.8, 141.9, 142.3, 142.4, 142.6, 142.8, 142.9, 143.1, 143.2, 143.3 (C_{60}-sp^2), 143.8, 143.9 (Ar-C), 144.2, 144.5, 144.7, 145.0 (C_{60}-sp^2), 155.3, 155.5, 156.7 (Ar-C), 163.5, 163.7, 166.9, 167.1, 172.5 ppm (C=O); IR (ATR): $\tilde{\nu} = 735$, 796, 900, 1092, 1216, 1228, 1365, 1435, 1508, 1738, 2341, 2360, 2970, 3004 cm^{-1}; UV/Vis (CH_2Cl_2): λ (log ε) = 260 (5.15), 320 (4.79), 426 (5.43), 518 (4.28), 594 (3.89), 651 nm (3.71); MS (FAB, NBA): *m*/*z*: 2595 [M^+], 2539 [M^+−*t*Bu], 2483 [M^+−2*t*Bu], 2427 [M^+−3*t*Bu], 720 [C_{60}^+].

Compound Zn^{II}-9: Compound **H_2-9** (100 mg, 0.04 mmol) and Zn-(OAc)$_2$2H_2O (44 mg, 0.20 mmol) were dissolved in $CHCl_3$ (50 mL) and heated at reflux for 3 h. Purification was carried out with column chromatography (SiO_2, CH_2Cl_2/ethyl acetate 8:2) and recrystallization from *n*-pentane. The product was obtained as a violet solid in 98% yield (104 mg). ^{1}H NMR (400 MHz, RT, $CDCl_3$): $\delta = 1.28$ (m, 32H; *t*Bu), 1.29 (m, 24H; *t*Bu), 1.85 (m, 6H; CH_2), 1.87 (m, 4H; CH_2), 2.07 (m, 10H; CH_2), 2.15 (m, 4H; CH_2), 3.91 (s, 6H; OCH_3), 4.35 (m, 4H; CH_2), 4.48 (m, 4H; CH_2), 4.76 (m, 2H; CH_2), 5.15 (m, 2H; CH_2), 6.56 (m, 1H; NH-(C=O)), 6.63 (m, 1H; NH(C=O)), 7.36 (m, 2H; Ar-H), 7.59 (m, 6H; Ar-H), 7.73 (m, 6H; Ar-H), 8.24 (m, 2H; Ar-H), 8.75 ppm (m, 8H; β-H); ^{13}C NMR (100.5 MHz, RT, $CDCl_3$,): $\delta = 28.0$, 28.1 (*t*Bu), 29.6, 29.6 (CH_2), 49.2 (CH_2), 53.9 (OCH_3), 57.7 (^{q}C), 65.1 (CH_2), 67.3 (CH_2), 67.5 (CH_2), 70.1, 70.7 (C^{60}-sp_3), 80.6 (^{q}C), 113.5, 115.1 (Ar-C), 120.3, 120.5, 121.0, 121.3 (*meso*-C), 123.4, 126.8, 127.6, 128.6, 128.6 (Ar-C), 131.9 (β-C), 137.7, 137.9, 138.1, 138.4, 139.5, 138.7, 139.5, 139.6, 140.0, 140.7, 140.7, 140.9, 141.1, 141.2, 141.3, 141.4, 141.6, 141.8, 141.9, 142.0, 142.3, 142.6, 142.8, 143.4 (C_{60}-sp^2), 143.5, 143.9 (Ar-C), 144.1, 144.7, 145.0, 147.9 (C_{60}-sp^2), 149.9, 150.1 (α-C), 155.2, 155.4, 156.6 (Ar-C), 163.4, 163.5, 167.0, 167.1, 172.4 ppm (C=O); IR (ATR): $\tilde{\nu} = 794$, 845, 889, 935, 1001, 1029, 1060, 1093, 1108, 1153, 1216, 1228, 1366, 1434, 1508, 1523, 1737, 2341, 2360, 2944, 2970, 3004 cm^{-1}; UV/Vis (CH_2Cl_2): λ (log ε) = 271 (5.28), 429 (5.48), 551 nm (4.32); MS (FAB, NBA): *m*/*z*: 2657 [M^+], 2320 [M^+−6*t*Bu], 720 [C_{60}^+].

Compound 3: Compound **6** (500 mg, 0.05 mmol) was dissolved in DMF (250 mL). After cooling the solution in an ice bath, DCC (380 mg, 1.84 mmol), HOBt (250 mg, 1.84 mmol), and DMAP (11 mg, 0.09 mmol) were added. The mixture was stirred for 1 h at 0 °C before **8** (1.98 g, 1.11 mmol) was added. After stirring for 3 d, the solvent was removed and the residual was dissolved in ethyl acetate. Precipitated DCU was removed by filtration and the solution was sequentially washed with solutions of citric acid (10%), $NaHCO_3$ (8%), brine, and water, and dried over $MgSO_4$. Adjacent purification by column chromatography (SiO_2, CH_2Cl_2/ethyl acetate 8:2) and recrystallization from *n*-pentane gave the red product in 64% (1.16 g) yield. ^{1}H NMR (400 MHz, RT, $CDCl_3$): $\delta = -2.85$ (br, 2H; NH), 1.35 (s, 162H; *t*Bu), 1.92 (m, 40H; CH_2), 2.14 (m, 56H; CH_2), 3.44 (s, 4H; CH_2), 3.67 (s, 6H; OCH_3), 4.39 (m, 4H; CH_2), 4.55 (m, 8H; CH_2), 6.10 (m, 6H; NH(C=O)), 7.32 (m, 2H; Ar-H), 7.33 (m, 2H; Ar-H), 7.60 (m, 6H; Ar-H), 7.66 (m, 6H; AR-H), 7.81 (m, 2H; Ar-H), 8.84 ppm (m, 8H; β-H); ^{13}C NMR (100.5 MHz, $CDCl_3$, RT): $\delta = 28.0$ (*t*Bu), 29.8, 29.9 (CH_2), 31.7, 31.9 (CH_2), 41.1 (CH_2), 52.5 (OCH_3), 57.5, 58.1 (qC), 63.8 (CH_2), 65.9 (CH_2), 67.4 (CH_2), 80.5 (^{q}C), 114.3, 115.3 (Ar-C), 119.5, 119.7, 120.3, 121.0 (*meso*-C), 127.6, 127.8, 128.1, 128.8 (Ar-C), 131.0 (β-C), 143.6, 155.7, 156.8 (Ar-C), 166.5, 166.7, 167.1, 172.3, 172.7 ppm (C=O); IR (ATR): $\tilde{\nu} = 735$, 781, 900, 1092, 1152, 1216, 1228, 1365, 1435, 1508, 1522, 1738, 2341, 2361, 2945, 2970, 3015 cm^{-1}; UV/Vis (CH_2Cl_2): λ (log ε) = 418 (5.56), 513 (4.21), 547 (3.83), 592 (3.83), 647 nm (3.83); MS (FAB, NBA): *m*/*z*: 3927 [M^+], 3871 [M^+−*t*Bu].

Compound H_2-10: C_{60} (110 mg, 0.15 mmol) were dissolved in toluene (300 mL) and degassed with argon for 15 min. Compound **3** (400 mg, 0.10 mmol) and iodine (105 mg, 0.40 mmol) were then added. DBU (62 μL, 0.40 mmol) dissolved in toluene (20 mL) was added dropwise over 30 min. After stirring for 2 d, the solution was concentrated and purified by column chromatography (SiO_2, toluene/ethyl acetate 1:1). Adjacent recrystallization from *n*-pentane yielded the product in 65% (308 mg) yield. ^{1}H NMR (400 MHz, RT, $CDCl_3$): $\delta = -3.05$ (br, 2H; NH), 1.33 (m, 162H; *t*Bu), 1.89 (m, 35H; CH_2), 2.13 (m, 61H; CH_2), 3.90 (m, 6H; OCH_3), 4.51 (m, 8H; CH_2), 4.77 (m, 2H; CH_2), 5.15 (m, 2H; CH_2), 6.04 (m, 6H; NH(C=O)), 7.26 (m, 2H; Ar-H), 7.55 (m, 2H; Ar-H), 7.63 (m, 6H; Ar-H), 7.74 (m, 6H; Ar-H), 8.23 (m, 2H; Ar-H), 8.67 ppm (m, 8H; β-H); ^{13}C NMR (100.5 MHz, RT, $CDCl_3$): $\delta = 28.0$ (*t*Bu), 29.8, 29.9 (CH_2), 31.7, 31.9 (CH_2), 49.1 (CH_2), 53.8 (OCH_3), 57.5, 58.1 (^{q}C), 65.0 (CH_2), 67.4 (CH_2), 67.6 (CH_2), 70.0, 70.7 (C_{60}-sp^3), 80.5 (^{q}C), 115.0, 115.4 (Ar-C), 119.6, 120.4 (*meso*-C), 123.8, 126.9, 127.8, 128.7 (Ar-C), 130.8 (β-C), 137.8, 138.0, 138.3, 139.1, 139.7, 139.9, 140.4, 140.9, 145.0, 141.1, 141.3, 141.5, 141.6, 141.8, 142.0, 142.3, 142.3, 142.4, 142.6, 143.2, 143.3 (C_{60}-sp^2), 143.6 (Ar-C), 143.9, 144.1, 144.5, 144.9, 147.8 (C_{60}-sp^2), 155.5, 155.9, 156.7, 156.9 (Ar-C), 163.5, 163.6, 167.7, 172.3, 172.7, 173.0 ppm (C=O); IR (ATR): $\tilde{\nu} = 734$, 797, 846, 900, 1105, 1152, 1216, 1228, 1366, 1455, 1508, 1523, 1737, 2341, 2360, 2945, 2970, 3004 cm^{-1}; UV/Vis (CH_2Cl_2): λ (log ε) = 260 (4.95), 320 (4.64), 426 (5.15), 517 (4.02), 551 (3.81), 592 (3.81), 645 nm (3.68); MS (FAB, NBA): *m*/*z*: 4643 [M^+], 4586 [M^+−*t*Bu], 720 [C_{60}^+].

Compound Zn^{II}-10: Compound **H_2-10** (150 mg, 0.03 mmol) and Zn-(OAc)$_2$2 H_2O (35 mg, 0.10 mmol) were dissolved $CHCl_3$ (50 mL) and heated to reflux for 3 h. After purification by column chromatography (SiO_2, CH_2Cl_2/ethyl acetate 6:4), the violet product was recrystallized from *n*-pentane and obtained in 73% (103 mg) yield. ^{1}H NMR (400 MHz, RT, $CDCl_3$): $\delta = 1.15$ (s, 28H; *t*Bu), 1.27 (s, 102H; *t*Bu), 1.39 (s, 32H; CH_2), 1.67 (m, 32H; CH_2), 1.93 (m, 52H; CH_2), 2.14 (m, 12H; CH_2), 3.90 (m, 6H; OCH_3), 4.51 (m, 8H; CH_2), 4.73 (m, 2H; CH_2), 5.16 (m, 2H; CH_2), 5.77 (m, 1H; NH(C=O)), 5.94 (m, 4H; NH(C=O)), 6.02 (m, 1H; NH(C=O)), 7.27 (m, 2H; Ar-H), 7.54 (m, 2H; Ar-H), 7.54 (m, 2H; Ar-H), 7.62 (m, 2H; Ar-H), 7.70 (m, 2H; Ar-H), 7.72 (m, 4H; Ar-H), 8.19 (m, 4H; Ar-H), 8.69 ppm (m, 8H; β-H); ^{13}C NMR (100.5 MHz, RT, $CDCl_3$): $\delta = 27.8$, 27.9, 28.1 (*t*Bu), 29.2, 29.5, 29.6, 29.8 (CH_2), 30.9, 31.7, 32.1 (CH_2), 49.1 (CH_2), 53.4 (OCH_3), 57.5, 57.7, 57.8 (^{q}C), 65.0 (CH_2), 67.2 (CH_2), 67.3 (CH_2), 67.0, 70.7 (C_{60}-sp^3), 80.5 (^{q}C), 115.0, 115.4 (Ar-C), 120.2 (*meso*-C), 123.8, 127.0, 127.4 (Ar-C), 131.4 (β-C), 137.9, 138.3, 138.8, 139.7, 140.0, 140.5, 140.9, 141.1, 141.3, 141.6, 141.8, 142.0, 142.3, 142.3, 143.0 (C_{60}-sp^2), 143.3 (Ar-C), 144.2, 144.4, 144.9, 145.1, 147.7 (C_{60}-sp^2), 149.7 (α-C), 155.2, 156.5 (Ar-C), 163.6, 163.7, 168.1, 172.3, 172.5, 172.7 ppm (C=O); IR (ATR): $\tilde{\nu} = 794$, 847, 952, 1000, 1106, 1152, 1216, 1228, 1366, 1435, 1455, 1522, 1737, 2341, 2360, 2944, 2970 cm^{-1}; UV/Vis (CH_2Cl_2): λ (log ε) = 260 (5.09), 318 (4.75), 433 (5.44), 555 nm (4.22); MS (FAB, NBA): *m*/*z*: 4706 [M^+], 4640 [M^+−*t*Bu], 4594 [M^+−2*t*Bu], 720 [C_{60}^+].

Water-soluble derivatives: General procedure for the synthesis of the water-soluble dendritic porphyrin-fullerene dyads: Dyads **M-9** (M = 2H) or **M-10** (M = Zn) were dissolved in 99% formic acid and stirred at room temperature for 24–36 h. The acid was evaporated, the residue was dissolved in THF or DMF, respectively, and recrystallized from *n*-pentane.

Compound ***H_2-11***: The brown product was isolated in 97% yield. ^{1}H NMR (400 MHz, RT, [D_8]THF): $\delta = -2.96$ (br, 2H; NH), 2.06 (m, 12H; CH_2), 2.25 (m, 12H; CH_2), 3.89 (m, 6H; OCH_3), 4.58 (m, 8H; CH_2), 4.78 (m, 2H; CH_2), 5.07 (m, 2H; CH_2), 6.82 (s, 1H; NH(C=O)), 6.99 (s, 1H; NH(C=O)), 7.47 (m, 6H; Ar-H), 7.64 (m, 4H; Ar-H), 7.78 (m, 2H; Ar-H), 7.84 (m, 2H; Ar-H), 8.28 (m, 2H; Ar-H), 8.73 ppm (m, 8H; β-H); ^{13}C NMR (100.5 MHz, RT, [D_8]THF): $\delta = 27.8$, 30.5 (CH_2), 50.6 (CH_2), 54.0 (OCH_3), 58.1 (CH_2), 71.2, 71.8 (C_{60}-sp^3), 114.4, 115.7 (Ar-C), 120.7, 122.0, 122.4 (*meso*-C), 127.3, 128.3, 128.6, 129.0 (Ar-C), 131.7 (β-C), 138.3, 138.7, 138.8, 138.9, 140.2, 140.4, 140.6, 140.7, 141.4,

141.6, 142.1, 142.4, 142.6, 142.6, 142.9, 143.2, 143.3, 143.6, (C_{60}-sp^2), 143.7, 143.9 (Ar-C), 144.5, 144.6, 145.4, 145.6 (C_{60}-sp^2), 157.2, 158.2 (Ar-C), 163.7, 167.3, 167.6, 174.5, 174.6 ppm (C=O); IR (ATR): $\tilde{\nu}$ = 728, 798, 917, 977, 1053, 1107, 1181, 1233, 1348, 1381, 1430, 1531, 1576, 1650, 1705, 1740, 2156, 2239, 2341, 2360, 2879, 2954, 3029 cm^{-1}; UV/Vis (H_2O): λ ($\log\varepsilon$) = 322 (4.67), 425 (5.14), 522 (4.07), 558 (3.80), 589 (3.75), 644 nm (3.51); MS (FAB, NBA): *m*/*z*: 2258 [M^+], 720 [C_{60}^+].

Compound ***H_2-12***: The product was obtained in 96% yield as a brown solid. ^{1}H NMR (400 MHz, RT, D_2O/[D_6]DMSO): δ = 1.73–2.00 (br, 96H; CH_2), 3.80 (br, 6H; OCH_3), 4.66–5.51 (br, 12H; CH_2), 7.02–8.63 ppm (br, 26H; Ar-H, β-H); ^{13}C NMR (100.5 MHz, RT, D_2O/[D_6]DMSO): δ = 29.6, 30.3, 31.2 (CH_2), 57.7 (^{q}C), 70.5 (C_{60}-sp^3), 143.7 (Ar-C), 174.0, 176.8 ppm (C=O); IR (ATR): $\tilde{\nu}$ = 729, 797, 887, 977, 1055, 1108, 1217, 1266, 1349, 1381, 1431, 1526, 1575, 1601, 1645, 1698, 1741, 2168, 2341, 2360, 2580, 2922, 2954, 3030 cm^{-1}; UV/Vis (H_2O): λ ($\log\varepsilon$) = 318 (4.49), 425 (5.04), 520 (3.93), 556 (3.75), 587 (3.62), 642 nm (3.45).

Compound ***Zn^{II}-11***: The product was gained in 98% yield as a violet solid. ^{1}H NMR (400 MHz, RT, [D_8]THF): δ = 2.05 (m, 12H; CH_2), 2.25 (m, 12H; CH_2), 3.92 (m, 6H; OCH_3), 4.54 (m, 8H; CH_2), 4.79 (m, 2H; CH_2), 5.12 (m, 2H; CH_2), 6.79 (s, 1H; NH(C=O)), 6.89 (s, 1H; NH(C=O)), 7.36 (m, 6H; Ar-H), 7.60 (m, 4H; Ar-H), 7.77 (m, 2H; Ar-H), 7.86 (m, 2H; Ar-H), 8.25 (m, 2H; Ar-H), 8.73 ppm (m, 8H; β-H); ^{13}C NMR (100.5 MHz, RT, [D_8]THF): δ = 28.5, 30.4 (CH_2), 50.5 (CH_2), 53.9 (OCH_3), 58.1 (CH_2), 71.1, 71.8 (C_{60}-sp^3), 114.0, 115.2 (Ar-C), 121.2, 121.3, 122.4 (*meso*-C), 127.5, 127.7, 127.9, 129.0 (Ar-C), 132.0 (β-C), 138.4, 138.8, 138.9, 139.0, 139.9, 140.6, 140.7, 141.5, 141.6, 142.1, 142.2, 142.3, 142.5, 142.6, 142.6, 142.9, 143.2, 143.6, (C_{60}-sp^2), 143.7, 143.9 (Ar-C), 144.6, 145.3, 145.4, 145.6, 145.7, 145.8, 146.0 (C_{60}-sp^2), 151.0, 151.1 (α-C), 156.8, 156.9, 157.9 (Ar-C), 162.1, 163.8, 167.2, 167.6, 174.5 ppm (C=O); IR (ATR): $\tilde{\nu}$ = 795, 888, 932, 1001, 1061, 1092, 1216, 1229, 1365, 1434, 1541, 1738, 2341, 2359, 2943, 2970, 3015 cm^{-1}; UV/Vis (H_2O): λ ($\log\varepsilon$) = 262 (5.25), 322 (4.77), 435 (5.25), 561 nm (4.19); MS (FAB, NBA): *m*/*z*: 2321 [M^+], 720 [C_{60}^+].

Compound ***Zn^{II}-12***: The product was obtained in 99% yield as a violet solid. ^{1}H NMR (400 MHz, RT, D_2O): δ = 1.85–2.41 (br, 96H; CH_2), 3.95 (br, 6H; OCH_3), 7.25–9.33 ppm (br, 26H; Ar-H, β-H); ^{13}C NMR (100.5 MHz, RT, D_2O): δ = 30.4, 31.1, 31.8, 32.0 (CH_2), 58.7 (^{q}C), 120.4 (*meso*-C), 128.5 (Ar-C), 131.9 (Ar-C), 140.8, 141.2, 141.6 (C_{60}-sp^2), 143.2 (Ar-C), 150.0, 150.1 (α-C), 165.3, 175.2, 175.4 ppm (C=O); IR (ATR): $\tilde{\nu}$ = 735, 793, 897, 999, 1093, 1206, 1216, 1228, 1365, 1455, 1488, 1557, 1647, 1738, 2341, 2360, 2945, 2970, 3016, 3446 cm^{-1}; UV/Vis (H_2O): λ ($\log\varepsilon$) = 262 (5.17), 317 (4.66), 435 (5.32), 559 nm (4.09); MS (FAB, NBA): *m*/*z*: 3695 [M^+].

Acknowledgements

Financial support by the German Science Foundation (DFG) through SFB 583 and the Excellence Cluster "Engineering of Advanced Materials" is gratefully acknowledged. We would like to thank Paul Bonnet explicitly for kindly providing the necessary data for the parameterization of the C_{60} fullerene for the employed AMBER force field.

[1] X. Camps, E. Dietel, A. Hirsch; S. Pyo, L. Echegoyen, S. Hackbarth, B. Röder, *Chem. Eur. J.* **1999**, *5*, 2362–2373; S. Pyo, L. Echegoyen, S. Hackbarth, B. Röder, *Chem. Eur. J.* **1999**, *5*, 2362–2373.
[2] P. J. Dandliker, F. Diederich, J.-P. Gisselbrecht, A. Louati, M. Gross, *Angew. Chem. Int. Ed. Engl.* **1996**, *34*, 2725–2728.
[3] P. J. Dandliker, F. Diederich, M. Gross, C. B. Knobler, A. Louati, E. M. Sanford, *Angew. Chem.* **1994**, *106*, 1821–1824; *Angew. Chem. Int. Ed. Engl.* **1994**, *33*, 1739–1842.
[4] P. J. Dandliker, F. Diederich, A. Zingg, J. P. Gisselbrecht, M. Gross, A. Louati, E. Sanford, *Helv. Chim. Acta* **1997**, *80*, 1773–1801.
[5] B. Felber, C. Calle, P. Seiler, A. Schweiger, F. Diederich, *Org. Biomol. Chem.* **2003**, *1*, 1090–1093.
[6] B. Felber, F. Diederich, *Helv. Chim. Acta* **2005**, *88*, 120–153.
[7] J.-F. Gnichwitz, M. Wielopolski, K. Hartnagel, U. Hartnagel, D. M. Guldi, A. Hirsch, *J. Am. Chem. Soc.* **2008**, *130*, 8491–8501.
[8] R. H. Jin, T. Aida, S. Inoue, *Chem. Commun.* **1993**, 1260–1262.
[9] C. Kovacs, A. Hirsch, *Eur. J. Org. Chem.* **2006**, 3348–3357.
[10] K. Maurer, K. Hager, A. Hirsch, *Eur. J. Org. Chem.* **2006**, 3338–3347.
[11] K. W. Pollak, J. W. Leon, J. M. J. Frechet, M. Maskus, H. D. Abruna, *Chem. Mater.* **1998**, *10*, 30–38.
[12] F. Wessendorf, J.-F. Gnichwitz, G. H. Sarova, K. Hager, U. Hartnagel, D. M. Guldi, A. Hirsch, *J. Am. Chem. Soc.* **2007**, *129*, 16057–16071.
[13] P. Weyermann, J.-P. Gisselbrecht, C. Boudon, F. Diederich, M. Gross, *Angew. Chem.* **1999**, *111*, 3400–3405; *Angew. Chem. Int. Ed.* **1999**, *38*, 3215–3219.
[14] A. Zingg, B. Felber, V. Gramlich, L. Fu, J. P. Collman, F. Diederich, *Helv. Chim. Acta* **2002**, *85*, 333–351.
[15] E. Dietel, A. Hirsch, E. Eichhorn, A. Rieker, S. Hackbarth, B. Roder, *Chem. Commun.* **1998**, 1981–1982.
[16] E. Dietel, A. Hirsch, J. Zhou, A. Rieker, *J. Chem. Soc. Perkin Trans. 2* **1998**, 1357–1364.
[17] D. M. Guldi, A. Hirsch, M. Scheloske, E. Dietel, A. Troisi, F. Zerbetto, M. Prato, *Chem. Eur. J.* **2003**, *9*, 4968–4979.
[18] D. M. Guldi, C. Luo, T. Da Ros, M. Prato, E. Dietel, A. Hirsch, *Chem. Commun.* **2000**, 375–376.
[19] D. M. Guldi, C. Luo, M. Prato, E. Dietel, A. Hirsch, *Chem. Commun.* **2000**, 373–374.
[20] D. M. Guldi, C. Luo, M. Prato, A. Troisi, F. Zerbetto, M. Scheloske, E. Dietel, W. Bauer, A. Hirsch, *J. Am. Chem. Soc.* **2001**, *123*, 9166–9167.
[21] J. Dannhäuser, W. Donaubauer, F. Hampel, M. Reiher, B. Le Guennic, B. Corzilius, K.-P. Dinse, A. Hirsch, *Angew. Chem.* **2006**, *118*, 3446–3450; *Angew. Chem. Int. Ed.* **2006**, *45*, 3368–3372.
[22] L. R. Sutton, M. Scheloske, K. S. Pirner, A. Hirsch, D. M. Guldi, J.-P. Gisselbrecht, *J. Am. Chem. Soc.* **2004**, *126*, 10370–10381.
[23] D. Balbinot, S. Atalick, D. M. Guldi, M. Hatzimarinaki, A. Hirsch, N. Jux, *J. Phys. Chem. B* **2003**, *107*, 13273–13279.
[24] T. Da Ros, M. Prato, *Chem. Commun.* **1999**, 663–669.
[25] P. Witte, F. Beuerle, U. Hartnagel, R. Lebovitz, A. Savouchkina, S. Sali, D. M. Guldi, N. Chronakis, A. Hirsch, *Org. Biomol. Chem.* **2007**, *5*, 3599–3613.
[26] F. Spaenig, M. Ruppert, J. Dannhaeuser, A. Hirsch, D. M. Guldi, *J. Am. Chem. Soc.* **2009**, *131*, 9378–9388.
[27] G. R. Geier III, J. S. Lindsey, *J. Chem. Soc. Perkin Trans. 2* **2001**, 677–686.
[28] J. S. Lindsey, K. A. MacCrum, J. S. Tyhonas, Y. Y. Chuang, *J. Org. Chem.* **1994**, *59*, 579–587.
[29] J. S. Lindsey, I. C. Schreiman, H. C. Hsu, P. C. Kearney, A. M. Marguerettaz, *J. Org. Chem.* **1987**, *52*, 827–836.
[30] J. Bernstein, H. L. Yale, K. Losee, M. Holsing, J. Martins, W. A. Lott, *J. Am. Chem. Soc.* **1951**, *73*, 906–912.
[31] A. McKillop, J. C. Fiaud, R. P. Hug, *Tetrahedron* **1974**, *30*, 1379–1382.
[32] G. R. Newkome, R. K. Behera, C. N. Moorefield, G. R. Baker, *J. Org. Chem.* **1991**, *56*, 7162–7167.
[33] G. R. Newkome, A. Nayak, R. K. Behera, C. N. Moorefield, G. R. Baker, *J. Org. Chem.* **1992**, *57*, 358–362.
[34] M. Brettreich, A. Hirsch, *Synlett* **1998**, 1396–1398.
[35] C. Bingel, *Chem. Ber.* **1993**, *126*, 1957–1959.
[36] J.-F. Nierengarten, V. Gramlich, F. Cardullo, F. Diederich, *Angew. Chem.* **1996**, *108*, 2242–2244; *Angew. Chem. Int. Ed. Engl.* **1996**, *35*, 2101–2103.
[37] J.-F. Nierengarten, J.-F. Nicoud, *Tetrahedron Lett.* **1997**, *38*, 7737–7740.
[38] M. Avalos, R. Babiano, J. L. Barneto, J. L. Bravo, P. Cintas, J. L. Jimenez, J. C. Palacios, *J. Org. Chem.* **2001**, *66*, 7275–7282.
[39] M. Avalos, R. Babiano, J. L. Barneto, P. Cintas, F. R. Clemente, J. L. Jimenez, J. C. Palacios, *J. Org. Chem.* **2003**, *68*, 1834–1842.
[40] T. Drakenberg, S. Forsen, *Chem. Commun.* **1971**, 1404–1405.

[41] D. Neuhaus, W. Williamson, *The Nuclear Overhauser Effect in Structural and Conformational Analysis*, VCH, Weinheim, **1989**.
[42] K. Stott, J. Keeler, Q. N. Van, A. J. Shaka, *J. Magn. Reson.* **1997**, *125*, 302–324.
[43] W. Bauer, A. Soi, A. Hirsch, *Magn. Reson. Chem.* **2000**, *38*, 500–503.
[44] A. D. Adler, F. R. Longo, F. Kampas, J. Kim, *J. Inorg. Nucl. Chem.* **1970**, *32*, 2443–2445.
[45] D. M. Guldi, K.-D. Asmus, *J. Phys. Chem. A* **1997**, *101*, 1472–1481.
[46] N. Carnieri, A. Harriman, *Inorg. Chim. Acta* **1982**, *62*, 103–107.
[47] For the ZnP-containing systems a splitting of the Q-bands was also discernable due to interactions between the deprotonated Newkome type dendrons and ZnP.
[48] A closer analysis of the differential absorption spectra at the conclusion of each of these time windows shows, however, the same radical ion pair state features.
[49] Such findings point to charge recombinations that are located in the strongly exothermic region of the Marcus parabola—exceeding 0.85 eV.
[50] A. Hirsch, I. Lamparth, H. R. Karfunkel, *Angew. Chem.* **1994**, *106*, 453; *Angew. Chem. Int. Ed.* **1994**, *33*, 437.

Received: March 26, 2010
Published online: July 28, 2010

